THE FASEB JOURNAL • RESEARCH • www.fasebj.org

An image-based small-molecule screen identifies vimentin as a pharmacologically relevant target of simvastatin in cancer cells

Kathryn P. Trogden,[*,1] Rachel A. Battaglia,[*,1] Parijat Kabiraj,[*] Victoria J. Madden,[†] Harald Herrmann,[‡,§] and Natasha T. Snider[*,2]

[*]Department of Cell Biology and Physiology and [†]Department of Pathology and Laboratory Medicine, University of North Carolina–Chapel Hill, Chapel Hill, North Carolina, USA; [‡]Division of Molecular Genetics, German Cancer Research Center, Heidelberg, Germany, and [§]Institute of Neuropathology, University Hospital Erlangen, Erlangen, Germany

ABSTRACT: Vimentin is a cytoskeletal intermediate filament protein that is expressed in mesenchymal cells and cancer cells during the epithelial-mesenchymal transition. The goal of this study was to identify vimentin-targeting small molecules by using the Tocriscreen library of 1120 biochemically active compounds. We monitored vimentin filament reorganization and bundling in adrenal carcinoma SW13 vimentin-positive (SW13-vim$^+$) cells *via* indirect immunofluorescence. The screen identified 18 pharmacologically diverse hits that included 2 statins—simvastatin and mevastatin. Simvastatin induced vimentin reorganization within 15–30 min and significant perinuclear bundling within 60 min (IC_{50} = 6.7 nM). Early filament reorganization coincided with increased vimentin solubility. Mevastatin produced similar effects at >1 μM, whereas the structurally related pravastatin and lovastatin did not affect vimentin. *In vitro* vimentin filament assembly assays revealed a direct targeting mechanism, as determined biochemically and by electron microscopy. In SW13-vim$^+$ cells, simvastatin, but not pravastatin, reduced total cell numbers (IC_{50} = 48.1 nM) and promoted apoptosis after 24 h. In contrast, SW13-vim$^-$ cell viability was unaffected by simvastatin, unless vimentin was ectopically expressed. Simvastatin similarly targeted vimentin filaments and induced cell death in MDA-MB-231 (vim$^+$), but lacked effect in MCF7 (vim$^-$) breast cancer cells. In conclusion, this study identified vimentin as a direct molecular target that mediates simvastatin-induced cell death in 2 different cancer cell lines.—Trogden, K. P., Battaglia, R. A., Kabiraj, P., Madden, V. J., Herrmann, H., Snider, N. T. An image-based small-molecule screen identifies vimentin as a pharmacologically relevant target of simvastatin in cancer cells. FASEB J. 32, 2841–2854 (2018). www.fasebj.org

KEY WORDS: statin · intermediate filaments · cytoskeleton · drug screen

The cytoskeleton, a critical structural element of all cells, is composed of intermediate filaments (IFs), actin filaments, and microtubules as its major components. Human IFs are encoded by 73 genes and grouped into 6 major types: types I–IV are cytoplasmic and include the epithelial and hair keratins, myocyte desmin, neurofilaments, and glial fibrillary acidic protein, among others; type V IFs are the nuclear lamins; and type VI are IFs expressed in the lens (1). Whereas pharmacologic agents that target actin filaments and microtubules are available and widely used in research, there are presently no known chemical probes that target IFs selectively. The importance of developing IF-targeting chemical probes is clear in light of what actin- and tubulin-targeting drugs have done for our fundamental understanding of cell biology and for patients with cancer. There are more than 70,000 PubMed studies that refer to the use of these agents, and microtubule drugs are a major class of chemotherapeutic agents (2, 3).

The complexity of IF assembly mechanisms and the limited structural data on individual IFs have hindered the development of pharmacologic tools for their targeting. All IF proteins share a common domain structure, a conserved coiled-coil rod domain that is flanked by globular head and tail domains (4). Stable IFs are assembled from tetramers, the basic IF subunits, into 10-nm-thick mature filaments that are critical for mechanical protection, stress sensing, and the regulation of transcription and cell growth. Presently, it is not known if and how the IF cytoskeleton mediates desired or untoward effects of clinically used drugs, despite the well-known functions of IFs in cellular homeostasis and disease.

Vimentin, the major IF protein of mesenchymal cells, has been used as a prototype for elucidating IF structure,

ABBREVIATIONS: IF, intermediate filament; MTT, methylthiazolyldiphenyltetrazolium bromide; PARP, poly(ADP-ribose) polymerase; Tx, Triton X-100

[1] These authors contributed equally to this work.

[2] Correspondence: Department of Cell Biology and Physiology, University of North Carolina–Chapel Hill, 5340C MBRB, 111 Mason Farm Rd., Chapel Hill, NC 27516, USA. E-mail: ntsnider@med.unc.edu

doi: 10.1096/fj.201700663R

This article includes supplemental data. Please visit *http://www.fasebj.org* to obtain this information.

Downloaded from www.fasebj.org by (75.189.134.82) on April 26, 2020. The FASEB Journal Vol. ${article.issue.getVolume()}, No. ${article.issue.getIssueNumber()}, pp. 2841-2854.

assembly, and dynamics (5). As such, vimentin can serve as a model IF protein to study pharmacologically relevant interactions between IFs and small-molecule compounds. Withaferin A, a naturally occurring steroidal lactone, has been used as a vimentin inhibitor on the basis of findings that it promotes aggregation of vimentin (6); however, withaferin A affects numerous cellular targets, including other cytoskeletal components (7, 8), and, therefore, it is not selective for vimentin or IFs in general. On the other hand, examining functional associations between IF proteins and compounds with well-defined biochemical activities may illuminate signaling networks controlling IF dynamics and set the stage for future development of novel first-in-class IF-selective chemical probes.

In the present study, we hypothesized that a pharmacologic screen using a library of compounds with known biochemical activities can provide us with new tools with which to manipulate IF structures, uncover signaling pathways that regulate IF dynamics, and potentially implicate IFs as biologically significant targets of widely used research compounds and clinical agents. We used Tocriscreen, a set of 1120 research compounds and clinical drugs, to screen for effects on vimentin filaments in a cell-based assay. This led to the identification of several hits that included compounds that target GPCRs, protein-protein interactions, and various classes of enzymes. We subsequently characterized a functional direct interaction between one of the hits, simvastatin, and vimentin. Simvastatin and other statins target the rate-limiting step in cholesterol synthesis and are among the most commonly used drugs in the world (9). In addition to lowering cholesterol, clinical use of statins is associated with reduced cancer mortality (10) and adverse muscle-related effects (11) through largely unknown mechanisms. Our identification of vimentin as a direct target of simvastatin provides a novel potential mechanism of action that extends beyond lowering cholesterol.

MATERIALS AND METHODS

Abs, plasmids, and chemicals

Abs used were rabbit anti-vimentin (total), pSer39, pSer56 and pSer83, total poly(ADP-ribose) polymerase (PARP) and cleaved PARP (Cell Signaling Technology, Danvers, MA, USA), mouse anti-vimentin V9, and tubulin DM1α (Sigma-Aldrich, St. Louis, MO, USA). Phalloidin (Molecular Probes, Eugene, OR, USA) was used to stain filamentous actin. Control, mEmerald-C1, and mEmerald-Vimentin-C-18 vectors were obtained from the Michael Davidson fluorescent protein collection (Addgene, Cambridge, MA). All chemicals used were purchased from Tocris (Bristol, United Kingdom), including the Tocriscreen screening set (a list of compounds is provided in Supplemental Table 1), in addition to individual lots of lovastatin, mevastatin, pravastatin, and simvastatin.

Cell cultures, immunofluorescence staining, imaging, and viability assay

Cell lines used in the study, SW13-vim$^+$, SW13-vim$^-$, MCF7, and MDA-MB-231, were cultured in DMEM with 10% fetal bovine serum, and 1% penicillin-streptomycin. For the small-molecule screen, cells were treated as described in the next section, then fixed with methanol and stained as previously described (12). Cells were imaged on the EVOS-FL auto cell imaging system (Thermo Fisher Scientific, Waltham, MA, USA) using a ×20 (0.75 NA) objective. For triple staining of actin, vimentin, and tubulin, cells were fixed in 4% paraformaldehyde for 10 min at room temperature, washed 3× in PBS, permeabilized in 0.1% Triton X-100 (Tx) for 5 min, washed 3× in PBS, and incubated in blocking solution (PBS/2.5% wt/vol bovine serum albumin). Primary Abs for vimentin (rabbit) and tubulin (mouse) were added overnight in 4°C. The next day, slides were washed 3× in PBS and incubated with Alexa Fluor–conjugated secondary Abs and phalloidin for 1 h at room temperature. After overnight mounting in ProLong Diamond (Thermo Fisher Scientific) that contained DAPI, cells were imaged on Zeiss 880 confocal laser scanning microscope using a ×63 (1.4 NA) oil immersion objective (Zeiss, Jena, Germany). Live/dead assays were performed by using the Ready Probes Cell Viability Imaging Kit (Molecular Probes). One drop of NucBlue (stains all cell nuclei) and NucGreen (stains dead cell nuclei) (both from Thermo Fisher Scientific) were added to the cells in 500 μl of culture medium 15 min before imaging. Cells were imaged in 24-well plates by using the EVOS-FL auto system with a ×10 (0.3 NA) objective. Quantification of nuclei from all cells (blue) and dead cells (green) was performed using the EVOS-FL autorecognition counting software. MTT (methylthiazolyldiphenyl-tetrazolium bromide) assay to determine cell viability on the basis of mitochondrial function was performed by using a commercial kit (Vybrant MTT; Thermo Fisher Scientific) according to the manufacturer's protocol.

Small-molecule screen, imaging, and quantification of vimentin filament changes

SW13-vim$^+$ cells were plated on 96-well glass-bottom plates and treated the following day (14 plates, 80 compounds per plate; 10 μM final drug added in serum-free DMEM). Each plate in the screen included 8 untreated and 8 vehicle (0.1% DMSO)-treated wells in serum-free DMEM as control. After 1 h of treatment, medium was aspirated and cells were fixed, stained, and imaged on the same day. Fixation and staining were performed as described in Snider *et al.* (12), and images were acquired on EVOS-FL auto using a ×20 objective (0.75 NA). Approximately 5% of the compounds caused cell liftoff, and they were not considered for additional analysis. The remaining wells were analyzed and scored manually for the appearance of the vimentin filament network (diffuse/nonfilamentous, peripheral redistribution, bundling, or aggregation). Compounds that produced one or more of these effects were considered positive hits, and all other compounds were considered negative hits in this screen. Quantification of vimentin-positive areas was performed by using ImageJ (National Institutes of Health, Bethesda, MD, USA). Vimentin-positive areas were calculated by using the analyze objects program with a size exclusion of <10 pixels^2. Raw images were converted to 8-bit images and the threshold was applied to remove background signal. Average vimentin area is defined as the total signal area of all objects divided by the number of objects in each image. The settings allowed the recognition of images >10 pixels^2 and the removal of nonspecific signal and signal from the edges.

Preparation of cell lysates and biochemical analysis of vimentin

Total cell lysates, Tx-soluble, and Tx-insoluble pellets or high-salt extracts (HSEs) were prepared as previously described (13).

Downloaded from www.fasebj.org by (75.189.134.82) on April 26, 2020. The FASEB Journal Vol. ${article.issue.getVolume()}, No. ${article.issue.getIssueNumber()}, pp. 2841-2854.

Two-dimensional gel electrophoresis samples were prepared in ReadyPrep buffer, which contained: 8M urea, 2% CHAPS, 50 mM DTT, 0.2% Bio-Lyte 3/10 ampholyte, 0.001% Bromophenol Blue (BioRad, Hercules, CA, USA) and subjected to isoelectric focusing: 250 V for 15 min, 8000 V for 2 h, 72,000 V hours, and 500 V hold. Cell lysates were resolved on 4–20% SDS-PAGE gels, then transferred to PVDF membranes. Membranes were blocked by using 5% milk in 0.1% Tween 20/PBS and incubated with the designated Abs in milk, with the exception of phospho-specific Abs, which were incubated in 3% bovine serum albumin in 0.1% Tween 20/PBS.

Electron microscopy

Recombinant human vimentin was generated as previously described (14), and vimentin filaments were assembled from tetramer buffer (5 mM Tris-HCL, pH 8.5, 1 mM EDTA, 1 mM DTT) using an established protocol (15) with an added 5-min preincubation step in the presence of vehicle or simvastatin. Vimentin filaments were negatively stained with 2% aqueous uranyl acetate (pH 4.5). A small droplet (2.5 μl) of protein suspension was applied to a glow-discharged formvar/carbon-coated 400 mesh copper grid and allowed to adsorb for 1–2 min. The grid was briefly floated on a droplet of deionized water to remove buffer salts and transferred to a droplet of 2% aqueous uranyl acetate for 30 s. Excess stain was removed by blotting with filter paper, and the grid was air dried. Grids were observed on a LEO EM 910 transmission electron microscope at 80 kV (Zeiss). Digital images were acquired by using a Gatan Orius SC1000 digital camera with Digital Micrograph software (v.2.3.1; Gatan, Pleasanton, CA, USA).

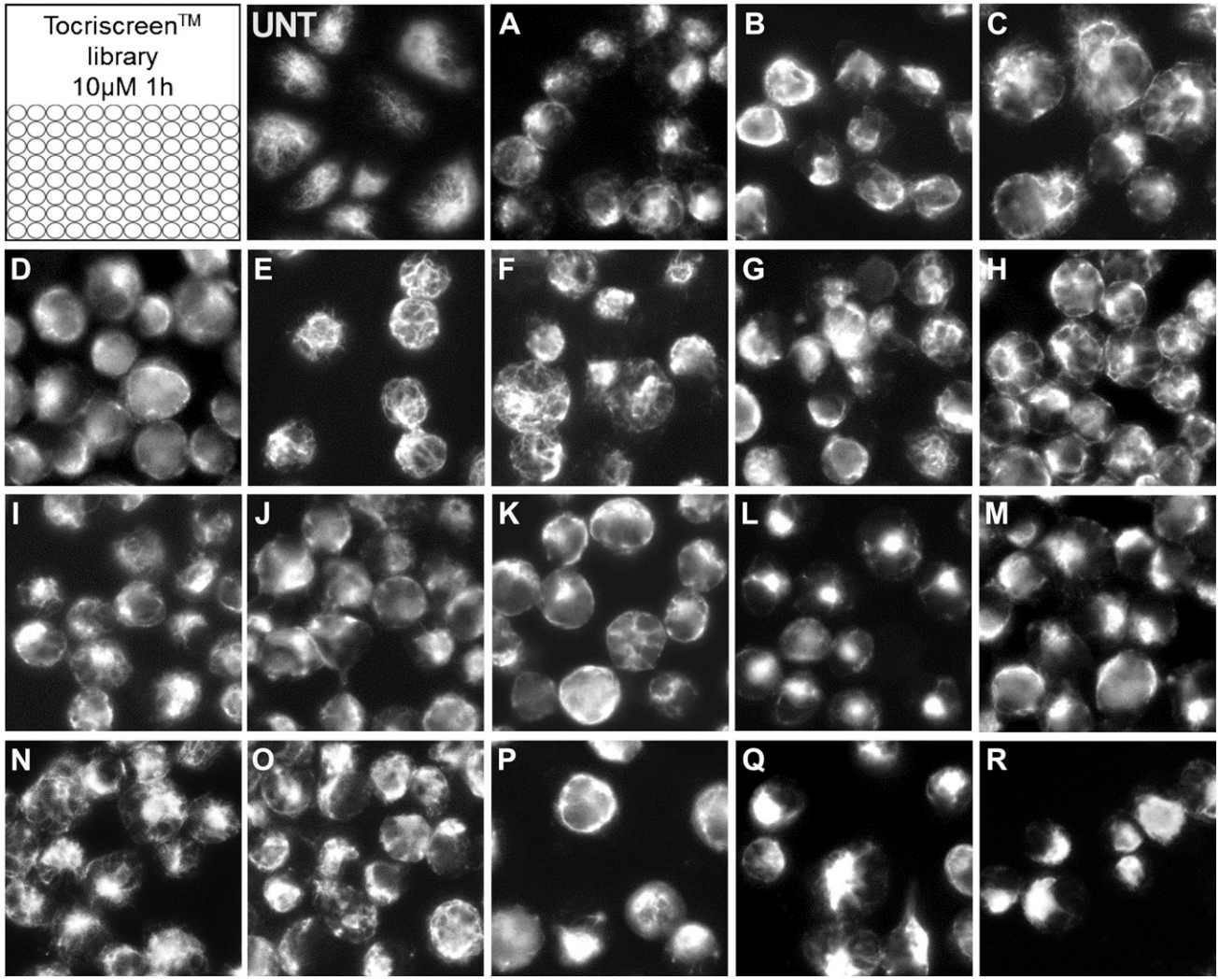

Figure 1. Image-based screen of 1120 biologically active small-molecule compounds for effects on vimentin filaments. SW13-vim$^+$ cells, plated on glass-bottom 96-well plates, were treated with 1 of 1120 different small-molecule compounds from the Tocriscreen library for 1 h, as described in Materials and Methods. Vimentin filaments were visualized in fixed cells by indirect immunofluorescence. Shown are untreated (UNT) cells and 18 positive hits. Positive hits are defined as those compounds that caused significant vimentin bundling, aggregation, and/or peripheral or cytoplasmic redistribution. Palmitoyl-carnitine chloride (*A*); cantharidin (*B*); CGP 52411 (*C*); *m*-3M3FBS (*D*); nocodazole (*E*); D-64131 (*F*); KF 38789 (*G*); diphenylene-iodonium chloride (*H*); LY 2183240 (*I*); carvedilol (*J*); SB 225002 (*K*); Ch 55 (*L*); INCA-6 (*M*); JK 184 (*N*); ivermectin (*O*); PNU 74654 (*P*); simvastatin (*Q*); and mevastatin (*R*). The compounds affect multiple targets and pathways, including: kinases, phosphatases, and lipases (*A–D*); microtubules and adhesion molecules (*E–G*); GPCRs and GPCR signaling (*H–K*); protein-protein interactions and multisubunit complexes (*L–P*); and cholesterol biosynthesis (*Q, R*). Note that some hits are expected (*e.g.*, nocodazole), whereas most hits are novel and unexpected, including simvastatin and mevastatin.

Downloaded from www.fasebj.org by (75.189.134.82) on April 26, 2020. The FASEB Journal Vol. ${article.issue.getVolume()}, No. ${article.issue.getIssueNumber()}, pp. 2841-2854.

RESULTS

Image-based small-molecule screen identifies vimentin-targeting compounds

We selected the Tocriscreen library because it consists of a collection of highly pure small molecules that are known to be biochemically active and that affect more than 300 pharmacologic targets, including GPCRs, kinases, ion channels, nuclear receptors, transporters, structural molecules, and protein complexes (a full compound list and known targets are included in Supplemental Table 1). We conducted the screen in SW13 adrenal carcinoma cells because these cells are commonly used in IF research and because of the availability of a vimentin-positive (SW13-vim$^+$) and a vimentin-negative (SW13-vim$^-$) clone, the latter lacking all cytoplasmic IFs (16). The pharmacologic screen—conducted as outlined in Materials and Methods—identified 18 positive hits that produced significant changes in vimentin filament morphology within 1 h of treatment (**Fig. 1** and **Table 1**). As a validation of the screening strategy, some of the positive hits we identified were expected on the basis of previous work, including kinase and phosphatase inhibitors and microtubule-targeting compounds. Among these, the PKC inhibitor, palmitoylcarnitine chloride (Fig. 1*A*), the PP1/PP2A inhibitor, cantharidin (Fig. 1*B*), and the microtubule depolymerizer, nocodazole (Fig. 1*E*), induced bundling and redistribution of vimentin filaments. We also identified several unexpected novel hits, such as diphenylene iodonium chloride (Fig. 1*H*) and LY 2183240 (Fig. 1*I*), which, among other activities, are known to target GPCR signaling related to cannabinoid actions and endocannabinoid signaling (17). Some of the most prominent and diverse effects on vimentin were observed when cells were treated with compounds that target protein-protein interactions and multisubunit complexes (Fig. 1*L–P*), which is relevant given the well-known scaffolding functions of vimentin and other IF proteins (18). We also observed striking vimentin bundling in the presence of simvastatin (Fig. 1*Q*) and mevastatin (Fig. 1*R*), 2 fungal metabolites that inhibit HMG-CoA, the rate-limiting enzyme in the cholesterol biosynthesis pathway (19). Mevastatin is not used in the clinic, whereas simvastatin and 2 related fungal-derived compounds, lovastatin and pravastatin (both included in the screening library), are commonly used for lowering cholesterol in patients (19). To validate and further explore mechanisms of the hits from the primary screen, we focused on statins because of their pharmacologic and clinical importance.

Simvastatin and mevastatin, but not lovastatin and pravastatin, cause dose-dependent bundling of vimentin IFs

The effects on vimentin filaments that were observed as part of the primary screen were confirmed by confocal

TABLE 1. *Positive hits and their corresponding primary targets*

Label	Compound	Primary target (compound activity)	Known functions of primary target
A	(±)-Palmitoylcarinitine chloride	PKC (inhibitor); membrane disruption	Context-dependent cell signaling functions
B	Cantharidin	PP1 and PP2A (inhibitor)	Context-dependent cell signaling functions
C	CGP 52411	EGFR (inhibitor)	Receptor tyrosine kinase regulating multiple signaling cascades
D	*m*-3M3FBS	PLC (activator)	Numerous cell signaling functions, including cytoskeletal dynamics
E	Nocodazole	Microtubule depolymerizer (inhibitor)	Cell division, movement, transport
F	D-64131	Microtubule depolymerizer (inhibitor)	Cell division, movement, transport
G	KF 38789	P-selectin mediated adhesion (inhibitor)	Cell adhesion molecule of endothelial cells and platelets
H	Diphenylene-iodonium chloride	GPR3 (agonist)	Orphan GPCR involved in aging, metabolism, and thermogenesis
I	LY 2183240	FAAH and anandamide uptake (inhibitor)	Endocannabinoid signaling
J	Carvedilol	β-Adrenergic receptor (antagonist)	GPCR targeted by catecholamines
K	SB 225002	CXCR2 chemokine receptor (antagonist)	GPCR targeted by IL-8 and CXCL1
L	Ch 55	RAR (agonist)	Regulation of gene expression
M	INCA-6	Calcineurin-NFAT interaction (inhibitor)	Gene regulation in response to environmental signals
N	JK 184	Hedgehog signaling (inhibitor)	Cell survival, differentiation, cancer
O	Ivermectin	α7-Nicotinic receptor (activator)	Ligand-gated calcium ion channel
P	PNU 74654	β-Catenin-TCF4 interaction (inhibitor)	Transcriptional regulation of cell adhesion and epithelial-mesenchymal transition
Q	Simvastatin	HMG-CoA reductase (inhibitor)	Cholesterol and nonsterol isoprenoid biosynthesis
R	Mevastatin	HMG-CoA reductase (inhibitor)	Cholesterol and nonsterol isoprenoid biosynthesis

CXCL1, C-X-C motif chemokine 1; CXCR2, C-X-C chemokine receptor type 2; EGFR, epidermal growth factor receptor; FAAH, fatty acid amide hydrolase; GPR3, G-protein coupled receptor 3; HMG-CoA, 3-hydroxy-3-methylglutaryl coenzyme A; NFAT, nuclear factor of activated T cells; RAR, retinoic acid receptor; TCF4, transcription factor 4.

Downloaded from www.fasebj.org by (75.189.134.82) on April 26, 2020. The FASEB Journal Vol. ${article.issue.getVolume()}, No. ${article.issue.getIssueNumber()}, pp. 2841-2854.

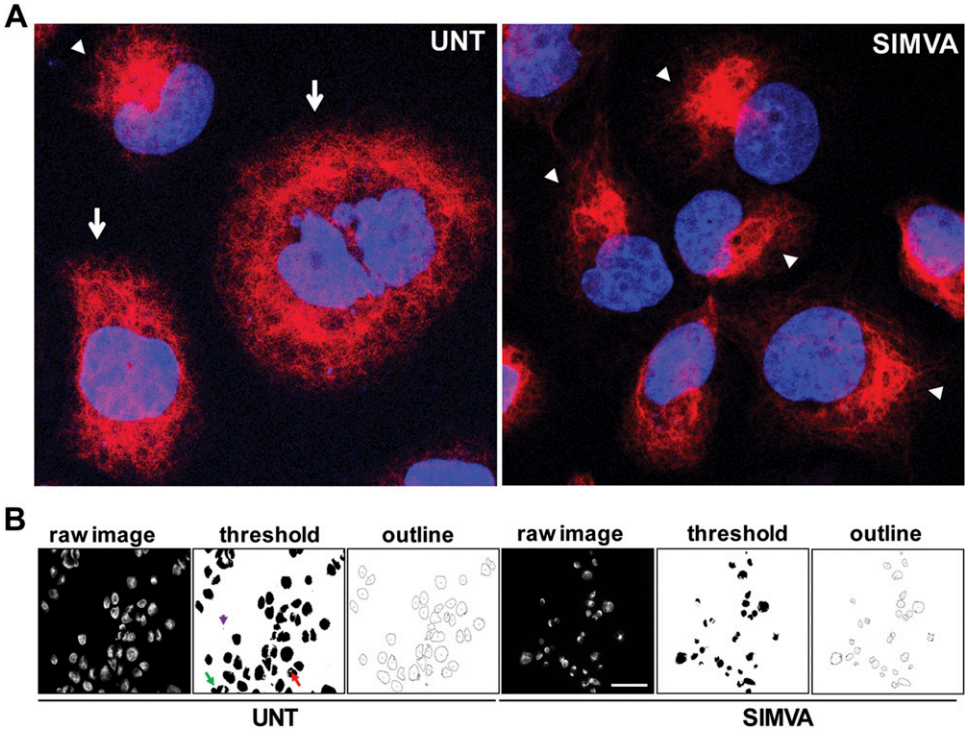

Figure 2. Quantification of drug-induced changes in vimentin filaments. *A*) Representative images of vimentin filaments (red) in untreated (UNT) and simvastatin (SIMVA)-treated SW13-vim$^+$ cells. Nuclei are stained with DAPI (blue). Vimentin filaments are marked by arrows and perinuclear vimentin bundles are marked by arrowheads. *B*) Quantification of the vimentin-positive area in the absence (UNT) and presence of drug; simvastatin is shown as a representative example. Shown is a raw image of vimentin staining, threshold of the raw images with black representing signal, and outlines of all objects recognized in the threshold image by the analyze particles program in ImageJ. The settings allowed for the recognition of images >10 pixels^2 to remove nonspecific signal (purple arrow), fill in holes (red arrow), and remove signal from the edges (green arrow).

imaging. Representative images in **Fig. 2*A*** show that simvastatin treatment caused the reorganization and bundling of vimentin filaments to one side of the nucleus in most cells (marked by arrowheads). Whereas some cells in the untreated group also exhibited a compact perinuclear ball-like vimentin structure, in the majority of untreated cells, vimentin filaments surrounded and extended away from the nucleus (Fig. 2*A*, arrows). To quantify the kinetics of vimentin bundling, we used ImageJ software to calculate the ratio of the total vimentin-positive area to the total number of objects (*i.e.*, cells), as described in Materials and Methods and shown in the representative images in Fig. 2*B*. We used this analysis tool to quantify the effects of 4 different statins on vimentin filaments. Simvastatin, mevastatin, pravastatin, and lovastatin were tested at concentrations of 1 nM–10 μM and 1 h of treatment. As

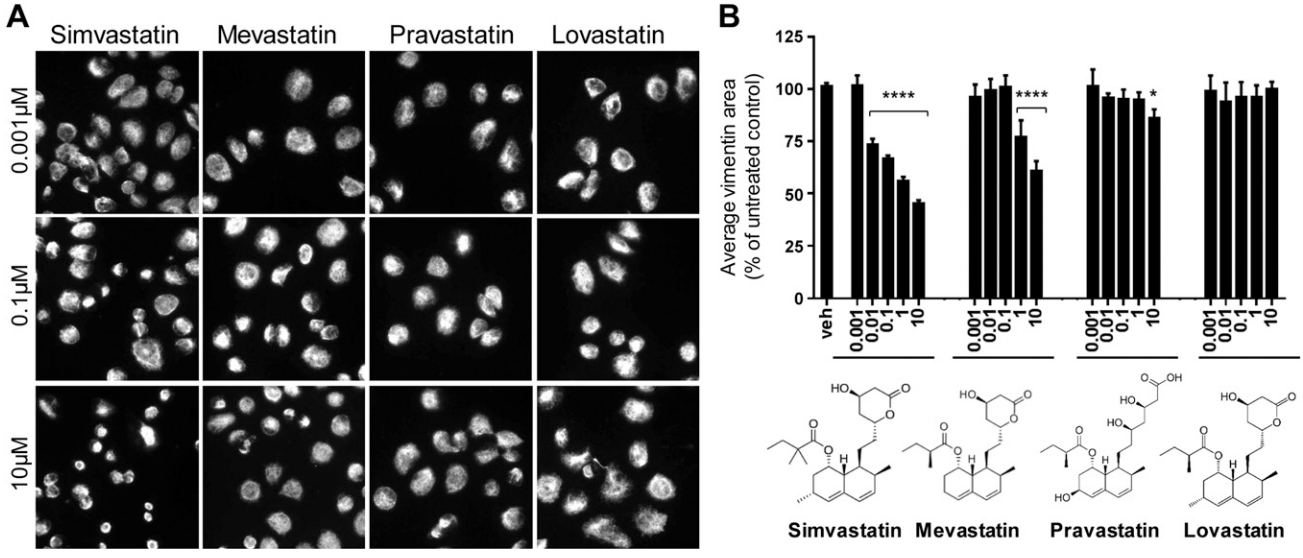

Figure 3. Dose-response effects of statins on vimentin filaments. *A*) Simvastatin, mevastatin, pravastatin, and lovastatin were applied for 1 h at concentrations that ranged from 0.001 to 10 μM. Note the dose-dependent decrease in the vimentin-positive area in response to simvastatin and mevastatin, but not pravastatin and lovastatin. Shown are representative images of 3 concentrations (0.001, 0.1, and 10 μM) from at least 3 independent experiments. *B*) Quantification of the total vimentin-positive area in cells that were treated with DMSO vehicle and the 4 statins (depicted structurally on the bottom) at different concentrations. Quantification was performed as described in Materials and Methods and Fig. 2*B*. *$P < 0.05$, ****$P < 0.0001$ relative to vehicle control (1-way ANOVA).

Downloaded from www.fasebj.org by (75.189.134.82) on April 26, 2020. The FASEB Journal Vol. ${article.issue.getVolume()}, No. ${article.issue.getIssueNumber()}, pp. 2841-2854.

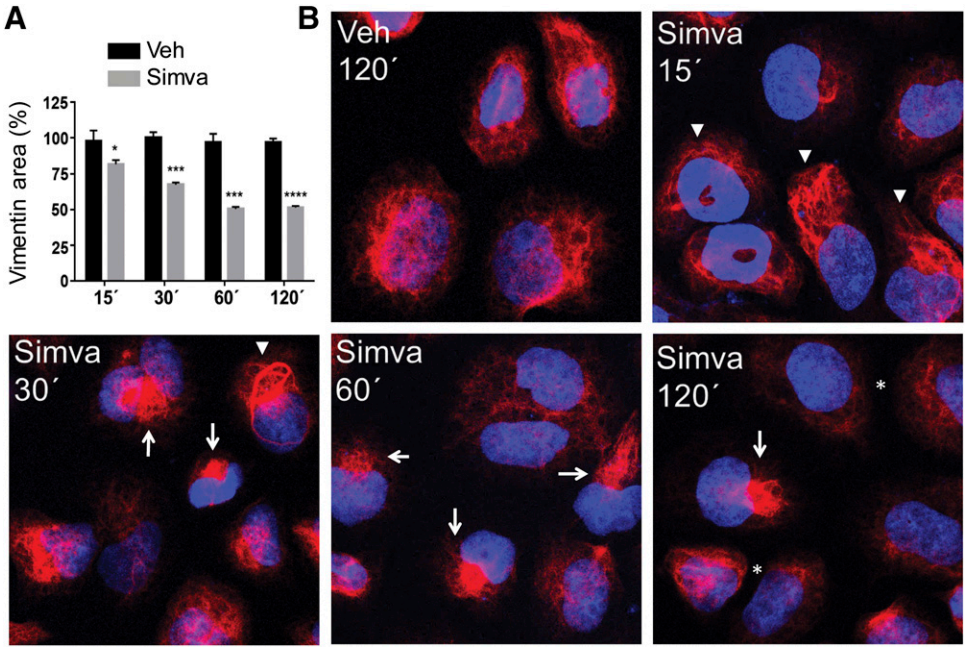

Figure 4. Time-dependent effects of simvastatin on vimentin in SW13 cells. *A*) Bar graph depicting time-dependent effects of simvastatin (gray bars) on the vimentin area relative to vehicle control (black bars). Both conditions are expressed as the percent of untreated control ($n = 3$ for each condition). *B*) Immunofluorescence images of vimentin (red) and DAPI (blue) at different time points after the addition of simvastatin (10 μM) or vehicle control. Vimentin filaments reorganize and shift to one side of the nucleus (arrowheads) after 15 min, followed by incorporation into ball-like perinuclear bundles at 30 and 60 min (arrows). At 120 min, many cells displayed diffuse nonfilamentous vimentin staining around the nuclei (asterisks). $*P < 0.05$, $***P < 0.001$, $****P < 0.0001$ (multiple Student's *t* tests).

shown **Fig. 3*A***, total vimentin area decreased significantly and dose dependently in response to simvastatin and mevastatin, but not lovastatin or pravastatin. Furthermore, whereas simvastatin was active at concentrations that ranged from 10 nM to 10 μM, mevastatin was less potent and affected vimentin only at concentrations ≥1 μM (Fig. 3*B*); therefore, we designed the next experiments to examine specifically the interaction between simvastatin and vimentin.

Simvastatin induces time-dependent vimentin bundling independently of changes on actin filaments and microtubules

We next assessed the vimentin bundling effects of simvastatin at several time points between 15 and 120 min. As shown in the bar graph in **Fig. 4*A***, the vimentin-positive area was reduced to 80, 67, and 50% of untreated control after 15, 30, and 60 min of simvastatin treatment, respectively. The

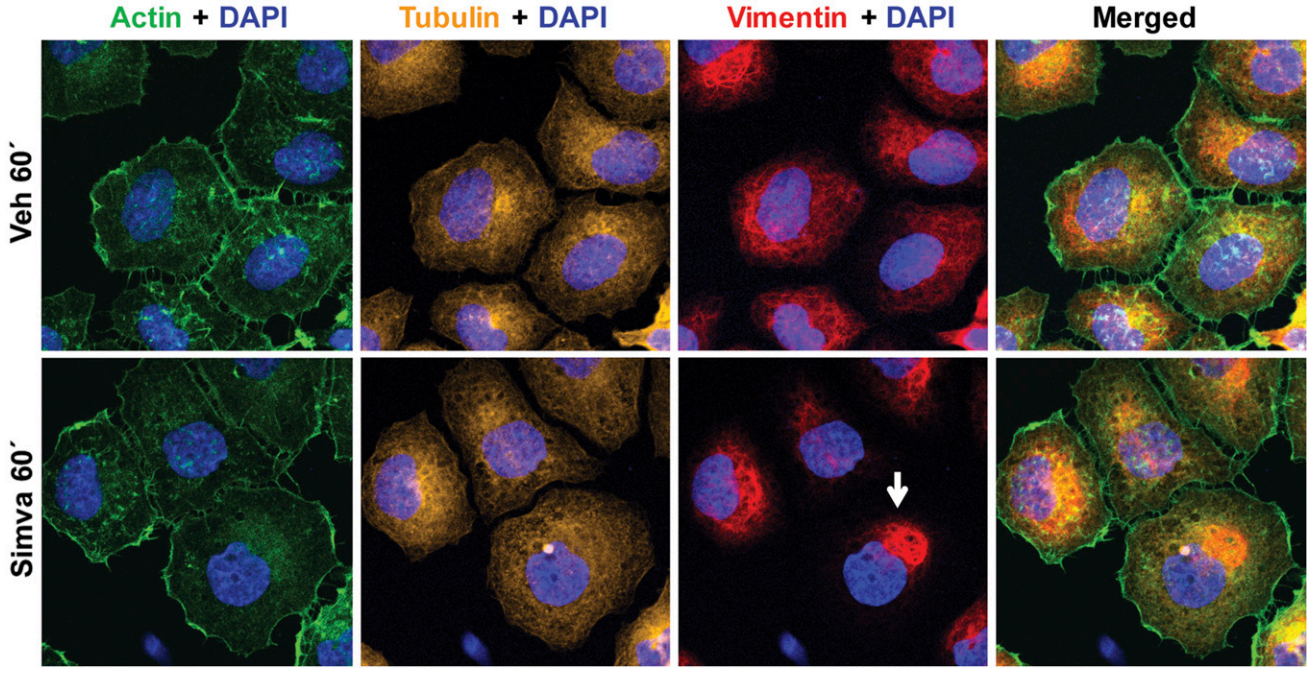

Figure 5. Comparison of simvastatin effects on actin filaments, microtubules, and vimentin filaments. Quadruple staining for actin (green) tubulin (orange), vimentin (red), and DNA (blue) in fixed SW13-vim$^+$ cells that were treated with vehicle (0.1% DMSO) or simvastatin (10 μM) for 60 min. Note the simvastatin-induced perinuclear vimentin bundling (arrow) and no changes in actin or tubulin. Shown are representative images of at least 3 independent experiments for each condition.

Downloaded from www.fasebj.org by (75.189.134.82) on April 26, 2020. The FASEB Journal Vol. ${article.issue.getVolume()}, No. ${article.issue.getIssueNumber()}, pp. 2841-2854.

maximal effect appeared after 60 min and was similar to the 120-min treatment. Representative confocal images in Fig. 4*B* indicate that, after 15 min, vimentin filaments reorganize and shift to one side of the nucleus (arrowheads), followed by the appearance of compact ball-like perinuclear vimentin bundles at 30 and 60 min (Fig. 4*B*, arrows). The rounded perinuclear bundles were also present in some cells after 120 min, although, at this time point, many cells displayed diffuse nonfilamentous vimentin staining surrounding the nucleus (Fig. 4*B*, asterisks). It has long been known that the inhibition of microtubule depolymerization causes vimentin to collapse to the perinuclear region of cells (20), a phenomenon we observed in our screen with 2 microtubule depolymerizing compounds—nocodazole and D-64131 (Fig. 1*E, F*). Microtubules act as tracks for the bidirectional transport of vimentin filaments to allow for a proper array (21). This link between microtubules and vimentin prompted us to explore whether simvastatin affected another cytoskeletal network, thereby indirectly changing vimentin organization. To answer this question, we simultaneously stained for actin, tubulin, and vimentin in cells that were treated with DMSO vehicle or simvastatin for 60 min (**Fig. 5**). At this time point, we did not observe significant changes to actin or tubulin, whereas perinuclear vimentin bundling (arrow) was as prominent as we had observed previously. These data indicate that simvastatin exhibits pharmacologic selectivity for vimentin over actin and tubulin.

Simvastatin causes time-dependent changes in vimentin solubility

We next examined how simvastatin affects the biochemical properties of vimentin. To study changes in solubility, we analyzed the presence of vimentin in the Tx-soluble fraction by immunoblot (**Fig. 6*A***), which revealed a 4-fold increase in Tx-soluble vimentin at 15–30 min after simvastatin treatment that returned to control levels at 60 min, as quantified in Fig. 6*B*. A corresponding 10–20% decrease of Tx-insoluble vimentin was observed after 15 and 30 min of treatment, with no significant difference at 60 min (Fig. 6*B*). The relative change in the Tx-insoluble pellet fraction was not as robust as the Tx-soluble fraction, as the bulk of vimentin is contained within the insoluble fraction (22). Because phosphorylation regulates vimentin dynamics (23), we examined whether simvastatin treatment altered vimentin phosphorylation at 3 common phosphorylation sites in the vimentin head domain (Ser39/-56/-83). As shown in Fig. 6*C*, we did not detect significant changes in site-specific phosphorylation either in the Tx-soluble fraction or in the insoluble high-salt extract; however, 2-dimensional gel analysis revealed an increase in the abundance of a negatively charged isoform of vimentin after 60 min of simvastatin treatment (Fig. 6*D*, arrow). This suggests that changes in vimentin phosphorylation at sites other than Ser39/-56/-83 or another post-translational modification accompany the morphologic changes in vimentin after 60 min of simvastatin treatment.

Simvastatin promotes vimentin bundling *in vitro*

We next examined the possibility that vimentin is a direct target of simvastatin. To test this possibility, we pre-incubated purified vimentin in tetramer buffer for

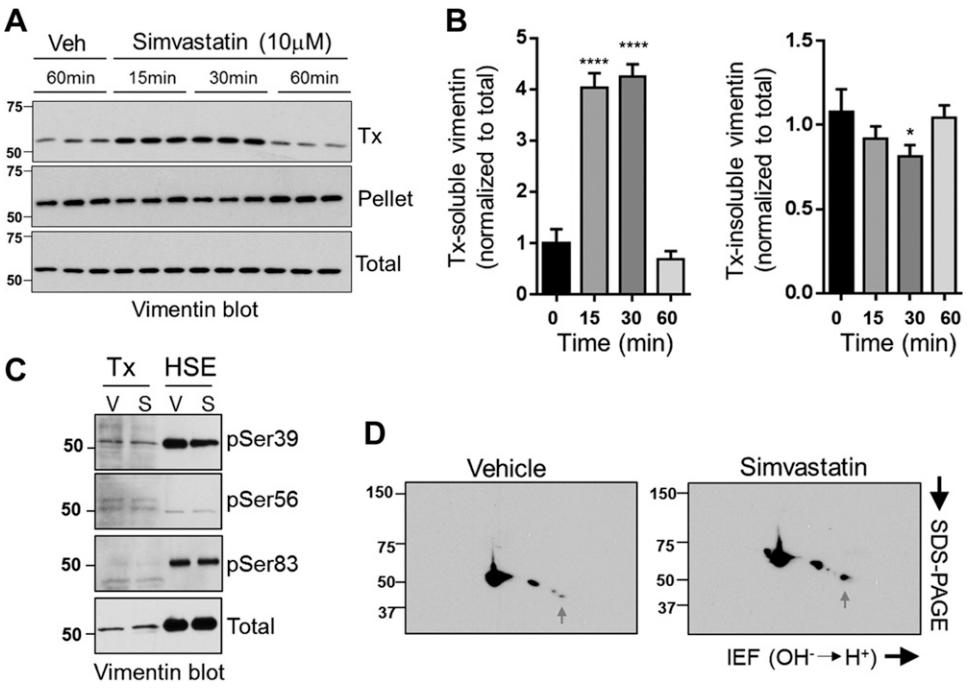

Figure 6. Biochemical characterization of the simvastatin effect on vimentin in SW13 cells. *A*) Comparison of vimentin levels in the Tx-soluble and -insoluble (pellet) fractions relative to total vimentin levels in response to simvastatin treatment for 15, 30, and 60 min. Each condition was assayed in triplicate, and shown are representative blots of at least 3 independent experiments. *B*) Quantification of the band intensity of the blots in panel *A*. $***P < 0.0001$, $*P < 0.05$ compared with control (1-way ANOVA). *C*) Immunoblot analysis of common vimentin phosphorylation sites in the presence and absence of simvastatin (10 μM; 60 min). *D*) Two-dimensional gel analysis of vimentin from DMSO vehicle- or simvastatin (10 μM, 60 min)-treated SW13-vim$^+$ cells. Note the increased abundance of negatively charged vimentin species (arrows) in the presence of simvastatin. HSE, high-salt extract.

Downloaded from www.fasebj.org by (75.189.134.82) on April 26, 2020. The FASEB Journal Vol. ${article.issue.getVolume()}, No. ${article.issue.getIssueNumber()}, pp. 2841-2854.

5 min in the presence of DMSO vehicle or simvastatin, initiated vimentin filament assembly, and allowed the reactions to proceed for 15, 30, or 60 min. Upon termination of the reactions, samples were pelleted at 100,000 *g*, and pellet fractions were analyzed by vimentin immunoblot, which revealed high-molecular-mass vimentin complexes (>250 kDa) in the presence of simvastatin (**Fig. 7*A***). Negative stain transmission electron microscopy analysis revealed bundling of vimentin filament precursors in the presence of simvastatin as early as 1 min after the initiation of assembly (Fig. 7*B*). The effect was more apparent on mature vimentin filaments (Fig. 7*C*). After 30 min of assembly, we observed the typical ~10-nm vimentin filaments, as well as ~20-nm-thick filaments in the presence of simvastatin, whereas after 60 min, we observed thick vimentin filament bundles that may correspond to the high-molecular-mass vimentin species that was detected biochemically upon simvastatin treatment in Fig. 7*A*. Of note, DMSO vehicle treatment itself promoted some bundling after 60 min, but this effect was relatively minor compared with the effect of simvastatin. Our *in vitro* studies indicate that vimentin is a direct target of simvastatin and suggest that this mechanism most likely accounts for the rapid simvastatin-induced reorganization and bundling of vimentin filaments that we observed in SW13-vim$^+$ cells.

Simvastatin, but not pravastatin, promotes vimentin-dependent cell death

To probe the functional significance of the simvastatin-vimentin interaction, we assessed whether simvastatin exerts different effects in SW13-vim$^+$ *vs.* SW13-vim$^-$ cells. After 24 h of simvastatin treatment, SW13-vim$^+$ cells became rounded with a corresponding drop off in cell number to <30% of control (**Fig. 8*A, B***). In contrast, simvastatin treatment did not affect the morphology or number of SW13-vim$^-$ cells (Fig. 8*A, B*). Pravastatin, which did not affect vimentin filaments (Fig. 3), also did not alter cell morphology or cell numbers in SW13-vim$^+$ cells (Fig. 8*C, D*). To probe this effect further, we assessed the dose dependency of simvastatin-induced cytotoxicity in SW13-vim$^+$ cells after 24 h of treatment. As shown in **Fig. 9*A***, simvastatin reduced the total number of SW13-vim$^+$ cells at submicromolar concentrations, with a corresponding IC_{50} of 48 nM (Fig. 9*C*). Furthermore, at low micromolar concentrations, simvastatin promoted significant induction of SW13-vim$^+$ cell death (Fig. 9*B, D*). We

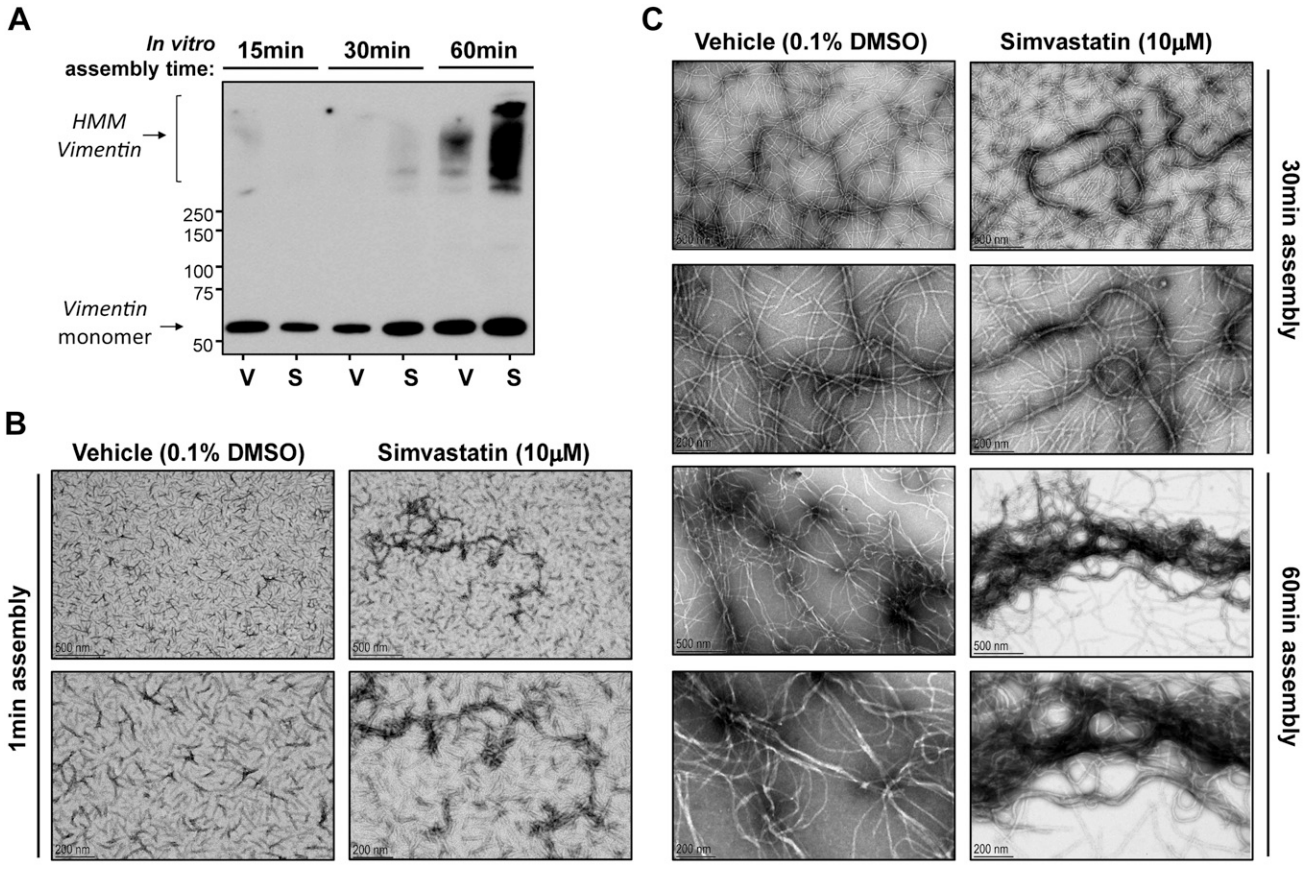

Figure 7. Effects of simvastatin on *in vitro*–assembled purified vimentin. *A*) Effect of 5-min, 10-μM simvastatin preincubation on purified vimentin after 15, 30, and 60 min in assembly reaction buffer. Note the time-dependent increase in high-molecular-mass (HMM) vimentin (>250 kDa) in the presence of simvastatin (S) compared with vehicle (V). *B*) Negative stain transmission electron microscopy (TEM) images of vimentin filament precursors after 1 min of reaction time showing simvastatin-induced vimentin bundling. *C*) TEM images of vimentin filaments after 30 and 60 min of assembly in the presence of DMSO or simvastatin. Note the presence of ~20-nm-thick vimentin filaments at 30 min and large vimentin bundles after 60 min.

Downloaded from www.fasebj.org by (75.189.134.82) on April 26, 2020. The FASEB Journal Vol. ${article.issue.getVolume()}, No. ${article.issue.getIssueNumber()}, pp. 2841-2854.

observed the 89-kDa caspase-3/-7 cleavage product of PARP in the simvastatin-treated SW13-vim$^+$ cells (Fig. 9*E*, *F*), which indicated that the cells were dying by apoptosis (24). Taken together, these results suggest that simvastatin targeting of vimentin may promote apoptotic cell death.

Ectopic vimentin overexpression sensitizes SW13-vim$^-$ cells to simvastatin

To determine conclusively whether simvastatin sensitivity of SW13-vim$^+$ cells is directly dependent on vimentin expression, we examined the response to simvastatin upon transient transfection of mEmerald-vimentin or mEmerald vector in SW13-vim$^-$ cells. Vimentin overexpression sensitized cells to simvastatin treatment, which resulted in a 50% drop off in cell number when vimentin was transiently overexpressed compared with vector alone (**Fig. 10*A***). Similar effects were observed upon stable vimentin overexpression, in which case simvastatin treatment caused a significant increase in the number of cells that contained rounded perinuclear vimentin bundles or aggregates (Fig. 10*B*, *C*). These effects mirror what we observed on endogenous vimentin in SW13-vim$^+$ cells and demonstrate that vimentin is a functionally relevant direct target of simvastatin that is critical for simvastatin-induced death in SW13 adrenal carcinoma cells.

Simvastatin targets vimentin filaments and causes cell death in MDA-MB-231 breast cancer cells

To determine whether our findings in SW13 cells extended to other cell types in which vimentin expression is known to regulate cellular properties, we tested 2 breast cancer cell lines: MCF7, which are vimentin deficient, and MDA-MB-231, which are vimentin expressing (**Fig. 11*B***). It has previously been shown that vimentin regulates properties that are related to the epithelial-mesenchymal transition in these cell lines (25). Similar to SW13 cells, vimentin filaments in MDA-MB-231 cells reorganized into perinuclear bundles in response to simvastatin (Fig. 11*A*). Furthermore, we observed significant cell death when MDA-MB-231 cells were treated with simvastatin, but not pravastatin (Fig. 11*C*). These data are also consistent with a published study that demonstrated that simvastatin induces cell death in MDA-MB-231 cells ($IC_{50} = 9$ μM), whereas pravastatin does not (26). We also quantified cell viability on the basis of the mitochondrial MTT assay, which revealed a ~40% decrease in viability in MDA-MB-231 cells (Fig. 11*D*). In contrast, vimentin-deficient MCF7 cells were not sensitive to either drug (Fig. 11*C*, *D*). Taken together, these results demonstrate that the findings in SW13 adrenal carcinoma cells translate to breast cancer cells in which vimentin is known to be functionally important.

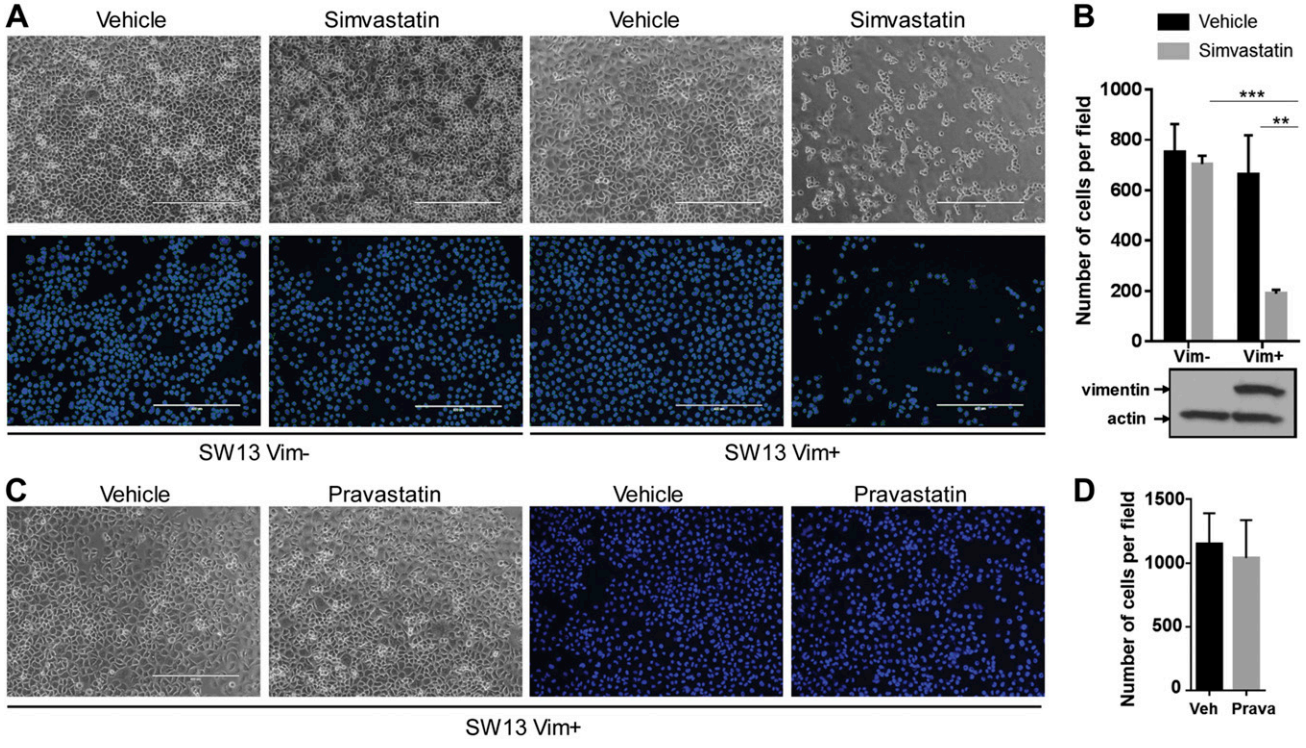

Figure 8. Simvastatin significantly inhibits the growth of SW13-vim$^+$ cells, but not SW13-vim$^-$ cells. *A*) Phase-contrast images (top) and nuclear stain (bottom) of SW13-vim$^-$ cells (left 4 panels) and SW13-vim$^+$ cells (right 4 panels). Note the decrease in the number of SW13-vim$^+$ cells in response to 24 h of simvastatin treatment (10 μM), appearing smaller and more rounded compared with vehicle-treated cells. *B*) Quantification of SW13 cell number after exposure to DMSO vehicle or 10 μM simvastatin for 24 h. Double immunoblot of actin and vimentin confirms vimentin presence and/or absence in cells. Data are representative of at least 3 independent experiments. *C*) Phase-contrast images and nuclear stain of SW13 vim$^+$ cells in response to 24 h of pravastatin treatment (10 μM), which does not affect cell morphology or viability. *D*) Quantification of SW13 cell number after exposure to DMSO vehicle or 10 μM pravastatin for 24 h. $^{**}P < 0.01$, $^{***}P < 0.001$ (2-way ANOVA).

Downloaded from www.fasebj.org by (75.189.134.82) on April 26, 2020. The FASEB Journal Vol. ${article.issue.getVolume()}, No. ${article.issue.getIssueNumber()}, pp. 2841-2854.

DISCUSSION

Intermediate filaments as novel drug targets

In the present study, we conducted a medium-throughput small-molecule screen that identified vimentin as a target for several known biochemically active small-molecule compounds. By using an image-based screen of the 1120-compound Tocriscreen library, we analyzed the effects on vimentin filaments after a relatively short exposure of 1 h to each test compound to minimize effects that may be secondary to other major cellular changes (*e.g.*, apoptosis or transcriptional reprogramming). With a small compound library, such as that used in this study, qualitative scoring for major reorganization of vimentin filaments was possible; however, future studies that involve larger compound libraries will necessitate the development of computational image analysis tools to monitor and quantify small changes in the IF network architecture that may be functionally relevant. A recent study that examined the interactions between vimentin filaments and microtubules is one example (27).

Vimentin as a pharmacologically relevant target of statins

Most of the novel hits we identified through the screen remain to be explored in detail, including the regulation of vimentin filaments by compounds that modulate GPCR signaling, protein-protein interactions, and enzymes that regulate post-translational modifications. An important future aspect of this work will be the subsequent

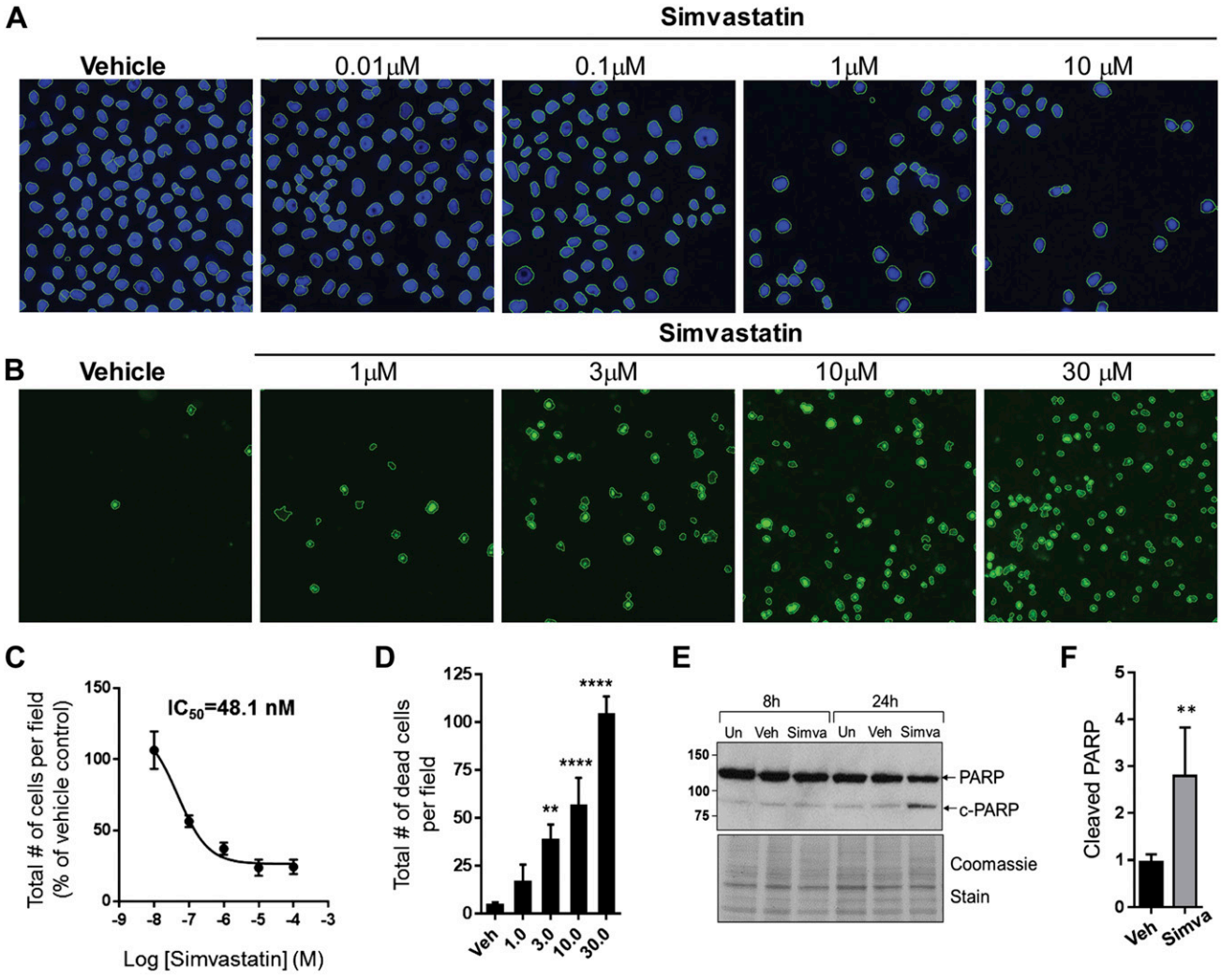

Figure 9. Simvastatin inhibits cell growth and induces dose-dependent apoptotic cell death in SW13-vim$^+$ cells. *A*) Simvastatin induces dose-dependent reduction in the total number of SW13-vim$^+$ cells at pharmacologically relevant concentrations (10 nM–10 μM). Blue stain marks the cell nuclei. Cell nuclei were circled (in green) and counted by using the EVOS-FL auto-count function. *B*) Simvastatin induces dose-dependent cell death in SW13-vim$^+$ cells. Green stain marks the nuclei of dead cells. All green nuclei were circled and counted by using the EVOS-FL auto-count function. *C*) Log dose-response curve for the total number of cells per field as a function of simvastatin dose, demonstrating inhibitory effects at low nanomolar concentrations (IC_{50} = 48.1 nM). *D*) Quantification of SW13-vim$^+$ cell death in the presence of different concentrations of simvastatin (micromolar). $^{**}P < 0.01$, $^{****}P < 0.0001$ compared with vehicle control; 1-way ANOVA. *E*) Western blot for full-length (~116 kDa) and cleaved (~89 kDa) PARP showing the presence of cleaved PARP after 24 h of simvastatin treatment. *F*) Quantification of cleaved PARP band from multiple immunoblots ($n = 5$). $^{**}P < 0.001$ (unpaired Student's *t* test).

Downloaded from www.fasebj.org by (75.189.134.82) on April 26, 2020. The FASEB Journal Vol. ${article.issue.getVolume()}, No. ${article.issue.getIssueNumber()}, pp. 2841-2854.

validation studies that involve dose-response and time-course experiments to discern which of the hits are pharmacologically relevant. On the basis of the novelty and potential clinical relevance, we focused here on the interaction between statins and vimentin. We demonstrate that simvastatin promotes vimentin filament bundling in the low nanomolar range, which is pharmacologically relevant as serum levels in patients who take statins are around 15 nM, with tissue exposure likely being higher (28). Our data suggest that the mechanism of action involves direct simvastatin-induced reorganization of vimentin filaments early on, followed by changes in vimentin post-translational modifications, and bundling at later time points, culminating in cell death (**Fig. 12**).

Simvastatin targeting of vimentin

Statins are taken by millions of people worldwide, and new treatment guidelines may significantly increase the number of patients who take them (9). The statins we tested are fungal metabolites that are related to the original statin (mevastatin), containing a hexahydronaphtalane ring (19). Simvastatin differs from lovastatin and pravastatin at the dimethylbutyrate ester side chain, which suggests that this functional group may be important for the activity on vimentin. Crystallographic data reveal that the presence of the additional methyl group on simvastatin affects the binding of simvastatin to *Aspergillus terreus* acyltransferase LovD (29, 30). Sequence alignment of LovD with human vimentin reveals 58% identify between the simvastatin-binding LovD peptide sequence, $_{267}$FGGQGVFSGPGS$_{278}$, and vimentin non–α-helical amino terminal (head) domain peptide, $_{15}$FGGPGTASRPSS$_{26}$. This suggests that the vimentin head domain may potentially mediate binding to simvastatin, although structural and mutagenesis studies will be required to elucidate the binding mechanism. Alternatively, the pharmacologic effects may be mediated *via* lipophilic interactions, as vimentin exhibits hydrophobic amino acid clusters and has previously been shown to have a high affinity for lipids (31).

Vimentin as a potential determinant of the sensitivity of cancer cells to simvastatin

Numerous prior studies have reported antiproliferative and proapoptotic effects of statins in cancer cells (32). Furthermore, previous observations across different cancer cell lines have demonstrated that sensitivity to statin-induced cell death correlates with high levels of vimentin expression (33). This bears significance as vimentin is a critical component of the epithelial-mesenchymal transition and regulates cell migration (34). Our dose-response studies reveal that simvastatin inhibits SW13 cell proliferation with an IC_{50} of 48 nM in vimentin-expressing, but not vimentin-lacking, cells. This demonstrates that the effects we observed at the cellular level occur at pharmacologically relevant concentrations and warrant additional investigation using *in vivo* models. It would also be of interest to analyze the effects of synthetic statins, such as fluvastatin, atorvastatin, and cerivastatin, on vimentin filament reorganization and vimentin-dependent cancer cell death. Our findings show that pravastatin differs from

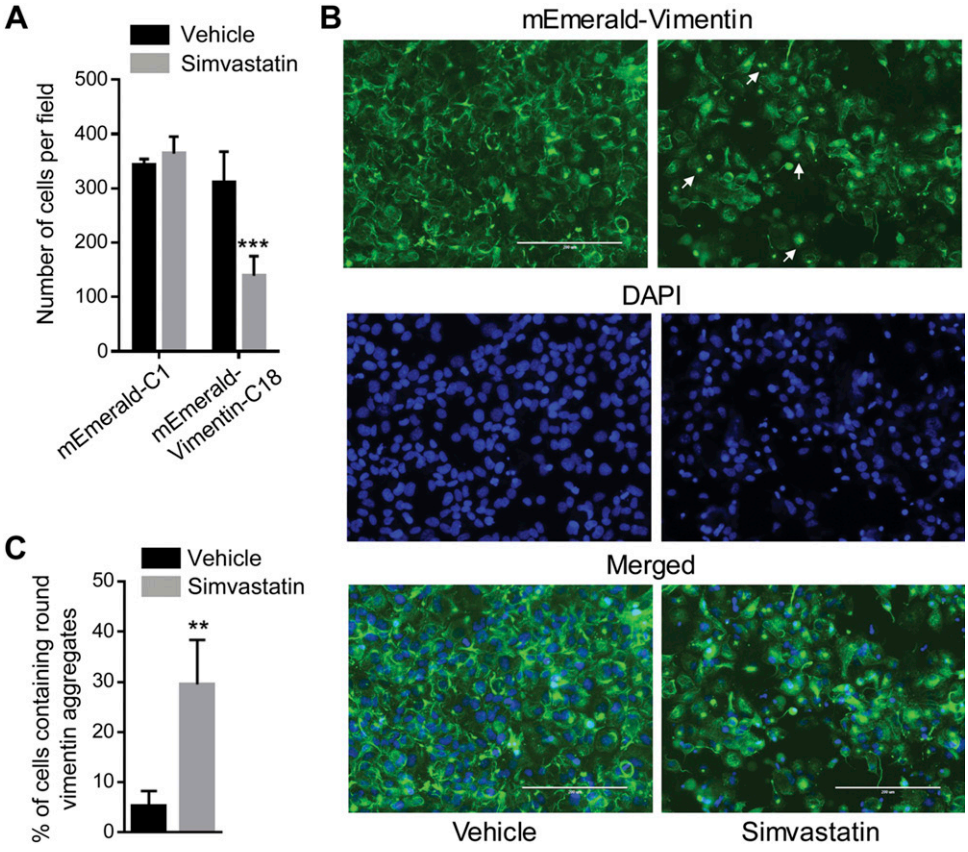

Figure 10. Ectopic expression of vimentin sensitizes SW13-vim$^-$ cells to simvastatin treatment. *A*) Transient overexpression of vimentin (24 h), followed by simvastatin treatment (10 μM, 24 h), promotes simvastatin-dependent cell death in SW13-vim$^-$ cells. *B*) Stable overexpression of mEmerald-vimentin sensitizes SW13-vim$^-$ cells to simvastatin treatment, which is accompanied by bundling and aggregation of mEmerald-vimentin. *C*) Quantification of the number of cells that contained vimentin bundles in the presence of vehicle or simvastatin. $^{**}P < 0.01$ (unpaired Student's *t* test), $^{***}P < 0.001$ relative to all other groups (2-way ANOVA).

Downloaded from www.fasebj.org by (75.189.134.82) on April 26, 2020. The FASEB Journal Vol. ${article.issue.getVolume()}, No. ${article.issue.getIssueNumber()}, pp. 2841-2854.

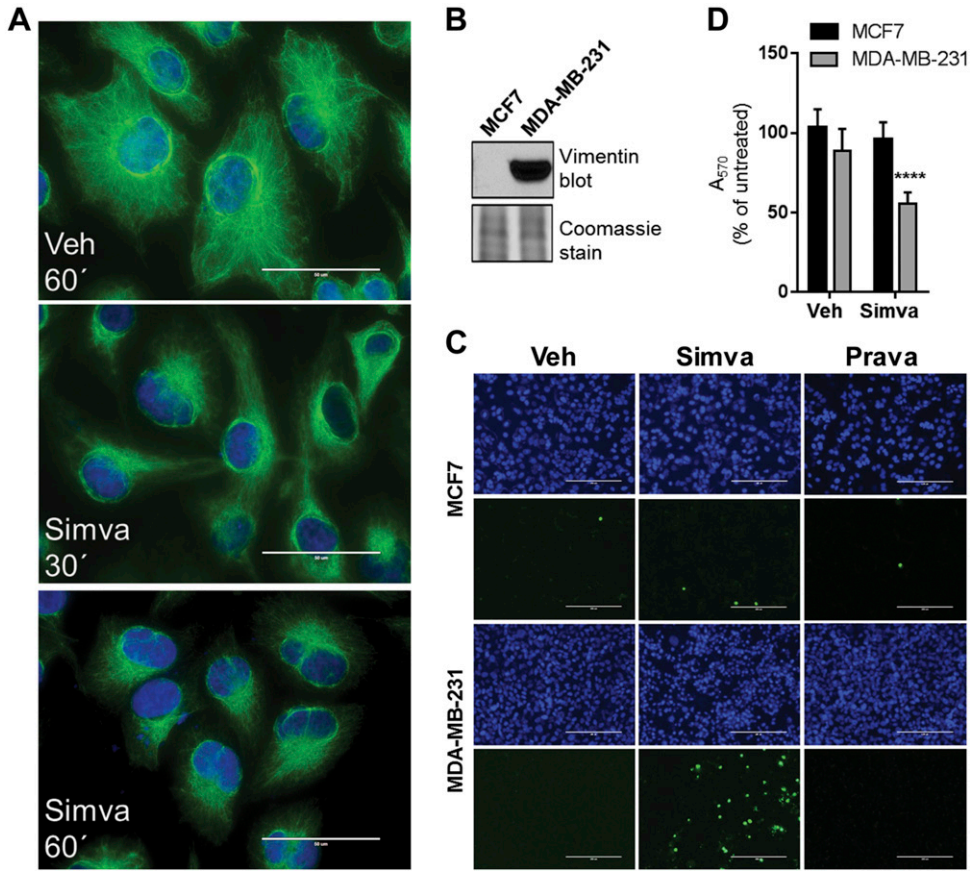

Figure 11. Simvastatin induces vimentin bundling and cell death in the vimentin-positive breast cancer cell line, MDA-MB-231. *A*) Morphology of vimentin filaments (green) in MDA-MB-231 cells treated with DMSO vehicle (top) or 10 μM simvastatin for 30 min (middle) or 60 min (bottom). Note the time-dependent perinuclear bundling of vimentin. Nuclei are stained with DAPI. Scale bar, 50 μm. *B*) Immunoblot of vimentin in MCF7 and MDA-MB-231 human breast cancer cells demonstrating the lack of vimentin in MCF7 cells. *C*) Live/dead staining showing the nuclei of all cells (blue) and dead cells (green). Note the increase in dead cells in the presence of simvastatin, but not pravastatin (10 μM; 24 h), in vimentin-expressing MDA-MB-231 cells. There is no increase in cell death in the vimentin-negative MCF7 in response to simvastatin or pravastatin. Scale bar, 200 μm. *D*) MTT assay (absorbance measurement at 570 nm) of MCF7 and MDA-MB-231 cells that were treated for 48 h in the presence of DMSO vehicle or 10 μM simvastatin ($n = 16$). ****$P < 0.0001$ (1-way ANOVA).

simvastatin in terms of its lack of effect on vimentin filaments and cell death in the lines tested. In a recent large, population-based cohort study, patients who received simvastatin had a 20% reduction in cancer-specific mortality, whereas use of pravastatin offered no protective benefit (35). The LUNGSTAR study, a multicenter phase III trial of pravastatin added to standard chemotherapy in small-cell lung cancer, concluded that there was no benefit of pravastatin (36). Furthermore, simvastatin has the most favorable profile on breast cancer prognosis, whereas preclinical and clinical studies have not supported a similar protective role of pravastatin (37).

Vimentin as a potential player in statin-associated muscle symptoms

Although desmin is the major IF in mature muscle fibers, vimentin is expressed during myogenesis and is increased during muscle injury (38, 39). Our results may also provide a potential mechanism for statin intolerance, a common clinical problem that limits the use of statins in a significant proportion of patients (40, 41). The molecular mechanisms of statin intolerance are poorly understood, and cytoskeletal and other structural or scaffolding proteins have not been implicated thus far (42); however, a previous study found a significant decrease in skeletal muscle mitochondrial DNA in patients who received simvastatin therapy (43). IFs, including vimentin, are critical regulators of intracellular organelles, including mitochondria (44, 45). Vimentin filaments specifically are known to regulate structural and functional aspects of mitochondria (46, 47), and the binding of mitochondria to vimentin is regulated by the small GTPase Rac1 (48). Because Rac1 is a known target of simvastatin in multiple cell types, including myoblasts, endothelial cells, and cancer cells (49, 50), it is plausible that vimentin may be an upstream mediator of the simvastatin effects on this pathway. The prevalence of muscle effects varies depending on the type of statin and correlates more strongly with simvastatin. In the Prediction of Muscular Risk in Observational conditions study, 18.2% of 1027 patients who received high-dose simvastatin therapy presented with muscular symptoms compared with 10.9% of 1901 patients who received high-dose pravastatin therapy (51). Our finding that simvastatin, but not pravastatin, targets vimentin IFs raises the possibility that the simvastatin-vimentin interaction bears potential significance to simvastatin action in muscle. Given the high degree of similarity between vimentin and desmin, it would be of particular interest to examine the effects of different statins on desmin IFs in future studies.

The need for pharmacologic tools to probe the function of vimentin and other intermediate filaments

Whereas many aspects of basic IF protein function and regulation were elucidated over the past 40 yr, much

Downloaded from www.fasebj.org by (75.189.134.82) on April 26, 2020. The FASEB Journal Vol. ${article.issue.getVolume()}, No. ${article.issue.getIssueNumber()}, pp. 2841-2854.

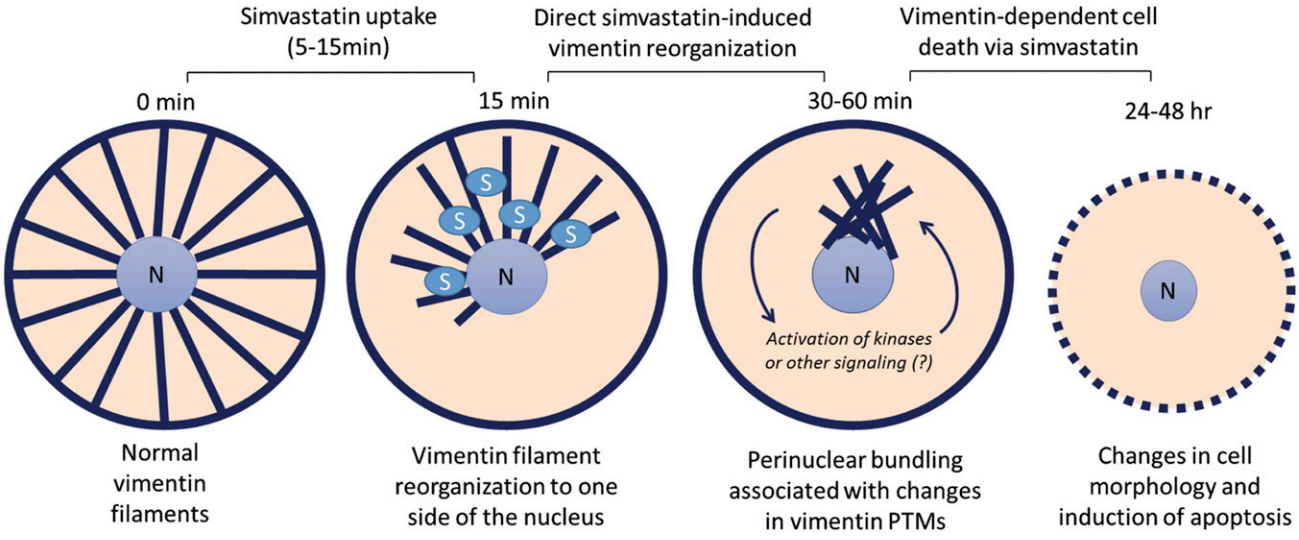

Figure 12. Proposed model for the mechanisms and consequences of vimentin targeting by simvastatin. Simvastatin promotes the reorganization of vimentin filaments to one side of the nucleus within 15 min of drug addition in SW13-vim$^+$ adrenal carcinoma cells. This timing is consistent with the known kinetics of simvastatin uptake in cells (52). Combined with the *in vitro* results that demonstrated that simvastatin directly affects vimentin filament assembly, this leads us to hypothesize that the early reorganization of vimentin filaments is a direct effect of simvastatin binding. Direct binding of simvastatin changes the biochemical properties of vimentin, which leads to increased solubility in Tx detergent buffer. At later time points after simvastatin addition (30–60 min), vimentin is organized into compact perinuclear bundles. This effect is observed in both SW13-vim$^+$ and MDA-MB-231 cells, and correlates with the sensitivity of these cells to simvastatin-induced apoptosis at later time points of 24–48 h. Cytotoxic effects are directly related to the combination of vimentin expression and simvastatin presence, as vimentin-lacking cells are not affected by simvastatin, and statins that do not affect vimentin (*e.g.*, pravastatin) fail to induce cell death in vimentin-expressing cells.

remains to be discovered. For example, mechanisms that underlie the crosstalk between IFs and other cytoskeletal systems, the identity and function of most IF-regulatory proteins, and the signaling pathways that mediate IF associations with the various cellular organelles are areas that lack in-depth understanding. Efforts to develop novel tool compounds to target IF proteins will accelerate our functional understanding of the IF cytoskeleton, which will open up new avenues for its pharmacologic manipulation in the clinic. To this end, the techniques and approaches used in the present study may be generally applicable to future small-molecule screens that aim to identify novel IF-selective compounds. FJ

ACKNOWLEDGMENTS

The authors thank Helen Willcockson and Deekshita Ramanarayanan (University of North Carolina–Chapel Hill) for technical assistance, and Dr. Susan J. Henning (University of North Carolina–Chapel Hill) for critical reading and helpful discussions of the manuscript. This work was supported by the Department of Cell Biology and Physiology at the University of North Carolina–Chapel Hill, The National Science Foundation Graduate Research Fellowship (to R.A.B), and by U.S. National Institutes of Health, National Institute of Diabetes and Digestive and Kidney Diseases Grant R01-DK110355 (to N.T.S.). The authors declare no conflicts of interest.

AUTHOR CONTRIBUTIONS

K. P. Trogden and N. T. Snider designed the research; K. P. Trogden, R. A. Battaglia, P. Kabiraj, V. J. Madden, and N. T. Snider performed the research; H. Herrmann contributed new reagents or analytic tools; and K. P. Trogden, R. A. Battaglia, H. Herrmann, and N. T. Snider analyzed the data and wrote the paper.

REFERENCES

1. Eriksson, J. E., Dechat, T., Grin, B., Helfand, B., Mendez, M., Pallari, H. M., and Goldman, R. D. (2009) Introducing intermediate filaments: from discovery to disease. *J. Clin. Invest.* **119**, 1763–1771
2. Cooper, J. A. (1987) Effects of cytochalasin and phalloidin on actin. *J. Cell Biol.* **105**, 1473–1478
3. Jordan, M. A., and Wilson, L. (2004) Microtubules as a target for anticancer drugs. *Nat. Rev. Cancer* **4**, 253–265
4. Herrmann, H., and Aebi, U. (2016) Intermediate filaments: structure and assembly. *Cold Spring Harb. Perspect. Biol.* **8**, a018242
5. Chernyatina, A. A., Guzenko, D., and Strelkov, S. V. (2015) Intermediate filament structure: the bottom-up approach. *Curr. Opin. Cell Biol.* **32**, 65–72
6. Bargagna-Mohan, P., Hamza, A., Kim, Y. E., Khuan Abby Ho, Y., Mor-Vaknin, N., Wendschlag, N., Liu, J., Evans, R. M., Markovitz, D. M., Zhan, C. G., Kim, K. B., and Mohan, R. (2007) The tumor inhibitor and antiangiogenic agent withaferin A targets the intermediate filament protein vimentin. *Chem. Biol.* **14**, 623–634
7. Vanden Berghe, W., Sabbe, L., Kaileh, M., Haegeman, G., and Heyninck, K. (2012) Molecular insight in the multifunctional activities of withaferin A. *Biochem. Pharmacol.* **84**, 1282–1291
8. Grin, B., Mahammad, S., Wedig, T., Cleland, M. M., Tsai, L., Herrmann, H., and Goldman, R. D. (2012) Withaferin a alters intermediate filament organization, cell shape and behavior. *PLoS One* **7**, e39065
9. Ioannidis, J. P. (2014) More than a billion people taking statins?: potential implications of the new cardiovascular guidelines. *JAMA* **311**, 463–464
10. Nielsen, S. F., Nordestgaard, B. G., and Bojesen, S. E. (2012) Statin use and reduced cancer-related mortality. *N. Engl. J. Med.* **367**, 1792–1802
11. Stroes, E. S., Thompson, P. D., Corsini, A., Vladutiu, G. D., Raal, F. J., Ray, K. K., Roden, M., Stein, E., Tokgözoğlu, L., Nordestgaard, B. G., Bruckert, E., De Backer, G., Krauss, R. M., Laufs, U., Santos, R. D., Hegele, R. A., Hovingh, G. K., Leiter, L. A., Mach, F., März, W., Newman, C. B., Wiklund, O., Jacobson, T. A., Catapano, A. L.,

Downloaded from www.fasebj.org by (75.189.134.82) on April 26, 2020. The FASEB Journal Vol. ${article.issue.getVolume()}, No. ${article.issue.getIssueNumber()}, pp. 2841-2854.

Chapman, M. J., and Ginsberg, H. N.; European Atherosclerosis Society Consensus Panel. (2015) Statin-associated muscle symptoms: impact on statin therapy—European Atherosclerosis Society Consensus Panel Statement on Assessment, Aetiology and Management. *Eur. Heart J.* **36**, 1012–1022
12. Snider, N. T., Leonard, J. M., Kwan, R., Griggs, N. W., Rui, L., and Omary, M. B. (2013) Glucose and SIRT2 reciprocally mediate the regulation of keratin 8 by lysine acetylation. *J. Cell Biol.* **200**, 241–247
13. Battaglia, R. A., Kabiraj, P., Willcockson, H. H., Lian, M., and Snider, N. T. (2017) Isolation of intermediate filament proteins from multiple mouse tissues to study aging-associated post-translational modifications. *J. Vis. Exp.* **123**, 1–16
14. Herrmann, H., Kreplak, L., and Aebi, U. (2004) Isolation, characterization, and *in vitro* assembly of intermediate filaments. *Methods Cell Biol.* **78**, 3–24
15. Kreplak, L., Richter, K., Aebi, U., and Herrmann, H. (2008) Electron microscopy of intermediate filaments: teaming up with atomic force and confocal laser scanning microscopy. *Methods Cell Biol.* **88**, 273–297
16. Sarria, A. J., Lieber, J. G., Nordeen, S. K., and Evans, R. M. (1994) The presence or absence of a vimentin-type intermediate filament network affects the shape of the nucleus in human SW-13 cells. *J. Cell Sci.* **107**, 1593–1607
17. Alexander, J. P., and Cravatt, B. F. (2006) The putative endocannabinoid transport blocker LY2183240 is a potent inhibitor of FAAH and several other brain serine hydrolases. *J. Am. Chem. Soc.* **128**, 9699–9704
18. Goldman, R. D., Grin, B., Mendez, M. G., and Kuczmarski, E. R. (2008) Intermediate filaments: versatile building blocks of cell structure. *Curr. Opin. Cell Biol.* **20**, 28–34
19. Goodman, L. S., Hardman, J. G., Limbird, L. E., and Gilman, A. G. (2001) *Goodman & Gilman's the Pharmacological Basis of Therapeutics*, McGraw-Hill, New York
20. Goldman, R. D. (1971) The role of three cytoplasmic fibers in BHK-21 cell motility. I. Microtubules and the effects of colchicine. *J. Cell Biol.* **51**, 752–762
21. Hookway, C., Ding, L., Davidson, M. W., Rappoport, J. Z., Danuser, G., and Gelfand, V. I. (2015) Microtubule-dependent transport and dynamics of vimentin intermediate filaments. *Mol. Biol. Cell* **26**, 1675–1686
22. Soellner, P., Quinlan, R. A., and Franke, W. W. (1985) Identification of a distinct soluble subunit of an intermediate filament protein: tetrameric vimentin from living cells. *Proc. Natl. Acad. Sci. USA* **82**, 7929–7933
23. Eriksson, J. E., He, T., Trejo-Skalli, A. V., Härmälä-Braskén, A. S., Hellman, J., Chou, Y. H., and Goldman, R. D. (2004) Specific in vivo phosphorylation sites determine the assembly dynamics of vimentin intermediate filaments. *J. Cell Sci.* **117**, 919–932
24. Chaitanya, G. V., Steven, A. J., and Babu, P. P. (2010) PARP-1 cleavage fragments: signatures of cell-death proteases in neurodegeneration. *Cell Commun. Signal.* **8**, 31
25. Mendez, M. G., Kojima, S., and Goldman, R. D. (2010) Vimentin induces changes in cell shape, motility, and adhesion during the epithelial to mesenchymal transition. *FASEB J.* **24**, 1838–1851
26. Jiang, P., Mukthavaram, R., Chao, Y., Nomura, N., Bharati, I. S., Fogal, V., Pastorino, S., Teng, D., Cong, X., Pingle, S. C., Kapoor, S., Shetty, K., Aggrawal, A., Vali, S., Abbasi, T., Chien, S., and Kesari, S. (2014) *In vitro* and *in vivo* anticancer effects of mevalonate pathway modulation on human cancer cells. *Br. J. Cancer* **111**, 1562–1571
27. Gan, Z., Ding, L., Burckhardt, C. J., Lowery, J., Zaritsky, A., Sitterley, K., Mota, A., Costigliola, N., Starker, C. G., Voytas, D. F., Tytell, J., Goldman, R. D., and Danuser, G. (2016) Vimentin intermediate filaments template microtubule networks to rnhance persistence in cell polarity and directed migration. *Cell Syst.* **3**, 252–263.e258
28. Björkhem-Bergman, L., Lindh, J. D., and Bergman, P. (2011) What is a relevant statin concentration in cell experiments claiming pleiotropic effects? *Br. J. Clin. Pharmacol.* **72**, 164–165
29. Jiménez-Osés, G., Osuna, S., Gao, X., Sawaya, M. R., Gilson, L., Collier, S. J., Huisman, G. W., Yeates, T. O., Tang, Y., and Houk, K. N. (2014) The role of distant mutations and allosteric regulation on LovD active site dynamics. *Nat. Chem. Biol.* **10**, 431–436
30. Gao, X., Xie, X., Pashkov, I., Sawaya, M. R., Laidman, J., Zhang, W., Cacho, R., Yeates, T. O., and Tang, Y. (2009) Directed evolution and structural characterization of a simvastatin synthase. *Chem. Biol.* **16**, 1064–1074
31. Traub, P., Perides, G., Scherbarth, A., and Traub, U. (1985) Tenacious binding of lipids to vimentin during its isolation and purification from Ehrlich ascites tumor cells. *FEBS Lett.* **193**, 217–221
32. Gazzerro, P., Proto, M. C., Gangemi, G., Malfitano, A. M., Ciaglia, E., Pisanti, S., Santoro, A., Laezza, C., and Bifulco, M. (2012) Pharmacological actions of statins: a critical appraisal in the management of cancer. *Pharmacol. Rev.* **64**, 102–146
33. Warita, K., Warita, T., Beckwitt, C. H., Schurdak, M. E., Vazquez, A., Wells, A., and Oltvai, Z. N. (2014) Statin-induced mevalonate pathway inhibition attenuates the growth of mesenchymal-like cancer cells that lack functional E-cadherin mediated cell cohesion. *Sci. Rep.* **4**, 7593
34. Kidd, M. E., Shumaker, D. K., and Ridge, K. M. (2014) The role of vimentin intermediate filaments in the progression of lung cancer. *Am. J. Respir. Cell Mol. Biol.* **50**, 1–6
35. Cardwell, C. R., Mc Menamin, Ú., Hughes, C. M., and Murray, L. J. (2015) Statin use and survival from lung cancer: a population-based cohort study. *Cancer Epidemiol. Biomarkers Prev.* **24**, 833–841
36. Seckl, M. J., Ottensmeier, C. H., Cullen, M., Schmid, P., Ngai, Y., Muthukumar, D., Thompson, J., Harden, S., Middleton, G., Fife, K. M., Crosse, B., Taylor, P., Nash, S., and Hackshaw, A. (2017) Multicenter, phase III, randomized, double-blind, placebo-controlled trial of Pravastatin added to first-line standard chemotherapy in small-cell lung cancer (LUNGSTAR). *J. Clin. Oncol.* **35**, 1506–1514
37. Ahern, T. P., Lash, T. L., Damkier, P., Christiansen, P. M., and Cronin-Fenton, D. P. (2014) Statins and breast cancer prognosis: evidence and opportunities. *Lancet Oncol.* **15**, e461–e468
38. Hamilton, S. M., Bayer, C. R., Stevens, D. L., Lieber, R. L., and Bryant, A. E. (2008) Muscle injury, vimentin expression, and nonsteroidal anti-inflammatory drugs predispose to cryptic group A streptococcal necrotizing infection. *J. Infect. Dis.* **198**, 1692–1698
39. Bryant, A. E., Bayer, C. R., Huntington, J. D., and Stevens, D. L. (2006) Group A streptococcal myonecrosis: increased vimentin expression after skeletal-muscle injury mediates the binding of *Streptococcus pyogenes*. *J. Infect. Dis.* **193**, 1685–1692
40. Fitchett, D. H., Hegele, R. A., and Verma, S. (2015) Cardiology patient page. Statin intolerance. *Circulation* **131**, e389–e391
41. Saxon, D. R., and Eckel, R. H. (2016) Statin intolerance: a literature review and management strategies. *Prog. Cardiovasc. Dis.* **59**, 153–164
42. Gluba-Brzozka, A., Franczyk, B., Toth, P. P., Rysz, J., and Banach, M. (2016) Molecular mechanisms of statin intolerance. *Arch. Med. Sci.* **12**, 645–658
43. Schick, B. A., Laaksonen, R., Frohlich, J. J., Päivä, H., Lehtimäki, T., Humphries, K. H., and Côté, H. C. (2007) Decreased skeletal muscle mitochondrial DNA in patients treated with high-dose simvastatin. *Clin. Pharmacol. Ther.* **81**, 650–653
44. Schwarz, N., and Leube, R. E. (2016) Intermediate filaments as organizers of cellular space: how they affect mitochondrial structure and function. *Cells* **5**, pii: E30
45. Lowery, J., Kuczmarski, E. R., Herrmann, H., and Goldman, R. D. (2015) Intermediate filaments play a pivotal role in regulating cell architecture and function. *J. Biol. Chem.* **290**, 17145–17153
46. Chernoivanenko, I. S., Matveeva, E. A., Gelfand, V. I., Goldman, R. D., and Minin, A. A. (2015) Mitochondrial membrane potential is regulated by vimentin intermediate filaments. *FASEB J.* **29**, 820–827
47. Tang, H. L., Lung, H. L., Wu, K. C., Le, A. H., Tang, H. M., and Fung, M. C. (2008) Vimentin supports mitochondrial morphology and organization. *Biochem. J.* **410**, 141–146
48. Matveeva, E. A., Venkova, L. S., Chernoivanenko, I. S., and Minin, A. A. (2015) Vimentin is involved in regulation of mitochondrial motility and membrane potential by Rac1. *Biol. Open* **4**, 1290–1297
49. Kou, R., Sartoretto, J., and Michel, T. (2009) Regulation of Rac1 by simvastatin in endothelial cells: differential roles of AMP-activated protein kinase and calmodulin-dependent kinase kinase-beta. *J. Biol. Chem.* **284**, 14734–14743
50. Zhu, Y., Casey, P. J., Kumar, A. P., and Pervaiz, S. (2013) Deciphering the signaling networks underlying simvastatin-induced apoptosis in human cancer cells: evidence for non-canonical activation of RhoA and Rac1 GTPases. *Cell Death Dis.* **4**, e568
51. Bruckert, E., Hayem, G., Dejager, S., Yau, C., and Bégaud, B. (2005) Mild to moderate muscular symptoms with high-dosage statin therapy in hyperlipidemic patients—the PRIMO study. *Cardiovasc. Drugs Ther.* **19**, 403–414
52. Atilano-Roque, A., and Joy, M. S. (2017) Characterization of simvastatin acid uptake by organic anion transporting polypeptide 3A1 (OATP3A1) and influence of drug-drug interaction. *Toxicol. In Vitro* **45**, 158–165

Received for publication July 14, 2017.
Accepted for publication December 26, 2017.

Downloaded from www.fasebj.org by (75.189.134.82) on April 26, 2020. The FASEB Journal Vol. ${article.issue.getVolume()}, No. ${article.issue.getIssueNumber()}, pp. 2841-2854.